NUMERICAL RAYTRACE VERIFICATION OF OPTICAL DIAGNOSTICS OF ICE SURFACE ROUGHNESS FOR INERTIAL CONFINEMENT FUSION EXPERIMENTS

JEFFREY A. KOCH,* THOMAS P. BERNAT, GILBERT W. COLLINS, BRUCE A. HAMMEL, ANDREW J. MacKINNON, and CHARLES H. STILL *University of California*
Lawrence Livermore National Laboratory P.O. Box 808, L-481, Livermore, California 94551

JAMES D. SATER and DONALD N. BITTNER *Schafer Corporation*
303 Lindbergh Avenue, Livermore, California 94550

Received May 14, 2001
Accepted for Publication November 26, 2001

Targets for future laser-fusion ignition experiments will consist of a frozen deuterium-tritium ice layer adhering to the inner surface of a spherical shell, and the specifications for the inner surface quality of this ice layer are extremely demanding. We have developed a numerical raytrace model in order to validate backlit optical shadowgraphy as an ice-surface diagnostic, and we have used the code to simulate shadowgraph data obtained from mathematical ice layers having known modal imperfections. We find that backlit optical shadowgraphy is a valid diagnostic of the mode spectrum of ice-surface imperfections for mode numbers as high as 80 provided the experimental data are analyzed appropriately. We also describe alternative measurement techniques, which may be more sensitive than conventional backlit shadowgraphy.

KEYWORDS: *laser fusion, cryogenic target, shadowgraphy*

I. INTRODUCTION

Ignition of thermonuclear burn in inertial confinement fusion (ICF) experiments[1] will require extremely precise control of many laser and target parameters. Targets currently envisioned for ignition experiments at the National Ignition Facility (NIF), a 192-beam laser under construction at Lawrence Livermore National Laboratory (LLNL), consist of a frozen deuterium-tritium (D-T) ice layer adhering to the inner surface of an ablator shell. The specifications for the inner surface quality of this ice layer are extremely demanding.[2,3] In order to achieve ignition on NIF, the D-T ice layer must be well characterized. In some target designs, the ablator shell is transparent to visible light, greatly facilitating ice-surface characterization, while in other designs the ablator shell is opaque.[1–3] Formation of suitably smooth ice layers in opaque shells will rely heavily on the experience gained from characterization of ice layers in transparent shells. Optical metrology of ice layers in transparent shells will therefore be critical to achieving ignition on NIF regardless of whether or not the ablator material is transparent, and reliable diagnostics are required.

Currently, the primary optical diagnostic of D-T ice surface quality in spherical shells is backlit shadowgraphy,[4] and the geometry of this technique is shown in Fig. 1. In this technique, light which is totally internally reflected from the inner ice surface is imaged in transmission as a bright band, and the power spectrum of the radial variations of the bright-band position is assumed to be equal to the power spectrum of the ice surface radial profile in the great-circle plane perpendicular to the shadowgraph optical axis. The one-dimensional root-mean-square (rms) roughness is obtained by summing the power spectrum coefficients.

The details of how the bright band maps to the inner ice surface are complex and depend on many factors. Earlier raytracing work examined the behavior of the bright-band position in the presence of localized surface imperfections, and found that the correlation depends on the height and curvature of the imperfection.[5] However, in general, a first-principles mathematical analysis is intractable, and raytracing utilizing localized surface imperfections does not obviously illuminate the general case of many coupled surface modes. In the present work we therefore take a different approach; we ignore the details

*E-mail: koch1@llnl.gov

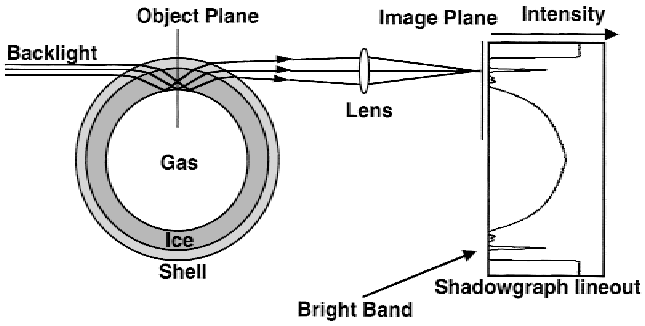

Fig. 1. Schematic of backlit shadowgraphy, illustrating how light totally internally reflected from the inner ice surface forms a bright band in transmission. Other ray groups form weaker inner bands near the bright band; these inner bands appear concentric and nearly circular when the ice surface is very smooth.

of how the local bright-band position correlates to individual imperfections, and instead we use exact numerical raytracing to examine how well the overall power spectrum derived from the bright-band analysis corresponds to the actual ice surface power spectrum inside the spherical shell. This approach directly addresses the validity of backlit shadowgraphy, since ignition capsules will ultimately be qualified against specifications on the basis of power spectra and rms measurements.

We considered experimental characterization of a fabricated surrogate capsule as an approach to validating shadowgraphy, but this approach presents significant difficulties. First, one must rely on calibrations from a separate inner-ice-surface diagnostic, which is known to be more reliable than shadowgraphy, and no such diagnostic exists over the full range of mode numbers accessible with shadowgraphy; raytracing through simulated capsules eliminates this problem by allowing mathematical ice surfaces to be specified to arbitrary precision. Second, an experiment would only allow validation with a single surrogate ice-surface profile, and other profiles would require separate surrogate shells to be fabricated; raytracing provides infinite flexibility for choice of simulated ice-surface parameters. Third, a diagnosable fabricated capsule would necessarily have different characteristics than a real ignition-qualifiable cryogenic ICF capsule (and would likely need to be a noncryogenic multilayer hemisphere), and the impact of these differences upon the conclusions of the experiments could not be known without raytracing to verify that the differences are quantifiable. Finally, a simulation capability allows alternative optical diagnostic techniques to be investigated and compared against shadowgraphy, and allows for detailed analysis of any subtleties which might arise.

We have therefore developed a nonsequential numerical raytrace code, SHELL3D, in order to address this issue.[6] With SHELL3D, we generate simulated ice surfaces with specified spherical-harmonic modal imperfections, and we produce simulated shadowgraphs which are interpreted with the same data analysis code used to interpret real experimental data. We find that shadowgraph-derived power spectra are reliable indicators of ice surface power spectra and total rms out to Fourier mode numbers as high as 80 *provided* the radial position of the bright band is defined with an appropriate fitting algorithm. We also find that the position fit previously used to define the bright band position in experimental data produces erroneously high power in the higher modes and overestimates the total rms by factors as large as 2; as a corollary, we find that experimentally produced ice surfaces are smoother than were once believed. Finally, we find that experimental diagnostic improvements may be obtained by changing the illumination geometry and analyzing other shadowgraph features and that enhanced information may be obtained by utilizing backlit transmission interferometry instead of simple backlit imaging. The results have significantly improved our understanding of how D-T ice surfaces may be characterized in order to qualify them for ICF experiments on NIF.

II. SIMULATING BACKLIT IMAGING DATA WITH SHELL3D

We begin by describing the operation of SHELL3D. The simulated capsule geometry is shown in Fig. 2. In SHELL3D, the outer and inner shell surfaces are defined as perfect cocentered spheres, and the inner ice surface

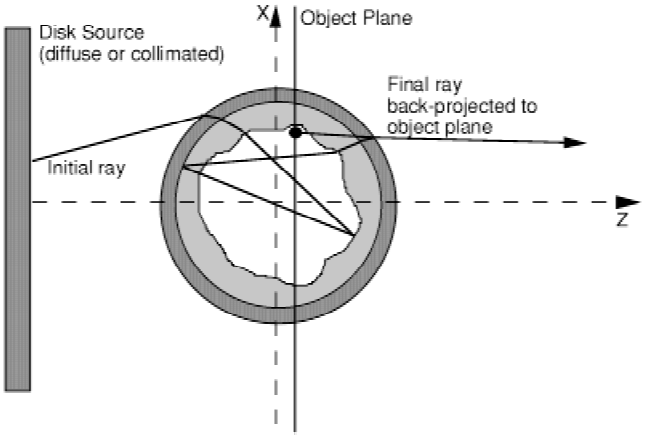

Fig. 2. Schematic of the raytracing geometry used in SHELL3D. The simulation is nonsequential in that each ray can reflect from or transmit through the surfaces in any order before leaving the capsule and being back-traced.

is defined as the sum of real-valued spherical harmonics with arbitrary values of l and m:

$$x^2 + y^2 + z^2 = R_1^2 \left[1 + \sum_{l=1} \left\{ \begin{array}{l} A_{l,0}\sqrt{2l+1}P_{l,0}(\cos\theta) \\ + \sum_{m=1}^{l} \sqrt{\frac{2(2l+1)(l-m)!}{(l+m)!}} P_{l,m}(\cos\theta)^* \\ (A_{l,m}\cos m\phi + A_{l,-m}\sin m\phi) \end{array} \right\} \right], \quad (1)$$

where R_1 is the $A_{0,0}$ coefficient, and the associated Legendre functions $P_{l,m}$ are defined by the usual recursion relations.[7,8] The outer ice surface is assumed identical to the inner shell surface, and the code does not permit topological changes such as cracks or gaps between the outer ice surface and the inner shell surface. Furthermore, each layer is assumed homogeneous and nonpolarizing. The x-axis in Fig. 2 is typically used for defining θ in the spherical harmonics, and all results discussed in this paper use this orientation. The assumption of a perfect shell is justifiable on the basis of rms shell roughness values which are ~100 times smaller than rms ice roughness values, both in ignition-acceptable target designs and in currently achievable surface qualities.[3] Finally, the neglect of features such as cracks and gaps is necessitated by the analytical approach of our SHELL3D model but is also justified by consideration that such features would primarily serve as local scattering sites, affecting the qualitative appearance of the images without causing significant deviations in ray trajectories. Large cracks and gaps are easily seen in experiments and are indicative of an ice layer which is very poor.

SHELL3D is essentially an analytical nonsequential raytracing code; starting from an initial source point (x_0, y_0, z_0) and an initial ray vector $\langle a, b, c \rangle$, the intersection point (x_1, y_1, z_1) with the outer surface $F(x, y, z) = 0$ is determined by substituting the parametric equations $F(x_0 + at, y_0 + bt, z_0 + ct) = 0$ and solving for t. The transmitted and reflected ray vectors are determined based on the incident vector, the surface normal $\nabla F(x_1, y_1, z_1)$, and the indices of refraction. The choice of reflection or transmission is probabilistic based on the ray polarization, angle of incidence, and indices of refraction; the process then repeats from the new point and ray vector, and continues until the ray leaves the capsule. Several features and subtleties are important to note:

1. The choice of spherical-harmonic recursion relations can have a significant impact on the numerical accuracy of the code, and, in particular, it is easy to generate spurious high-frequency structure near the poles ($\theta \approx 0$ and π) when using recursion relations that involve the term $\sqrt{1-\cos^2\theta}$ in the denominator. We have taken care to eliminate these instabilities from our algorithms, which arise from round-offs and divide-by-zero errors.

2. The polarization of each ray is randomly chosen and fixed as S or P. In fact, the polarization with respect to the local surface will generally evolve as the ray propagates through the capsule if the inner ice surface is not spherical. This effect is not treated in the code, but the practical result of this simplification will be negligible for nearly smooth surfaces.

3. A wrapped transmitted phase map is generated along with the image array, and this map can be postprocessed by phase-unwrapping software in order to generate a transmitted wavefront map, as will be discussed in Sec. IV.

4. The maximum number of surfaces each ray can intersect is 16. This is sufficient to pass all forward-scattered, twice-reflected rays.

5. The effective imaging lens is perfect and has no distortion but can be specified to have an effective point-spread function. In all cases discussed here, the imaged plane is the midplane of the capsule.

6. For the spherical surfaces, intersection points are determined analytically; there are generally two roots for each intersection, and the correct choice can be determined logically. For the spherical-harmonic surface, there are an unknown number of intersection points which cannot be determined analytically and which fall in an unknown order. For this surface, the code instead propagates the ray forward in small incremental steps in the region of the inner ice surface[a] until the first root is passed; this bounds the position of the root, which is then determined iteratively using an implementation of Brent's algorithm.[8]

The output shadowgraph array is a 1024 × 1024 pixelized image, which can be analyzed as if it were real data by the same analysis code, LAYER (Ref. 9), which is used to analyze experimental bright-band data. For comparison to the bright-band-derived power spectrum and surface rms calculated by LAYER, a separate code calculates the actual radial variations of the mathematically generated ice surface[b] as a function of θ in the great-circle plane perpendicular to the shadowgraph axis, and Fourier-transforms $\Delta R(\theta)$ to obtain a one-sided power spectrum. In both cases, the Fourier-mode coefficients sum to the square of the rms surface deviation in one dimension, which in turn can be related

[a] The region of the inner ice surface is defined by two spheres which entirely contain the ice surface profile; raytracing within this region must be done carefully to avoid possible errors caused by multiple intersection points.

[b] We calculate the great-circle-plane, one-dimensional power spectrum numerically using the same spherical-harmonic algorithms which are used in SHELL3D; this approach minimizes the potential impact of numerical errors in the algorithms on the comparison with the bright-band-derived power spectra.

to the two-dimensional rms power spectrum most relevant to ICF ignition capsule simulations.[10]

All codes currently run on DEC 8400 computers. The CPU time required to produce simulated images through two-dimensionally rough ice surfaces with SHELL3D scales approximately as L^2, where L is the maximum cutoff mode number. Good signal-to-noise ratios (>10 throughout the full field of view) for $L = 40$ can be obtained after ~750 CPU hours. For such large problems, multiple versions of SHELL3D can be run simultaneously using different random number seeds, and the results can be added to minimize the actual clock time required.

III. SHELL3D VALIDATION OF D-T ICE DATA

We described preliminary results obtained using a simplified rotationally symmetric version of SHELL3D in an earlier paper[6]; here we describe more recent results we obtained using the full capabilities of the code to validate real experimental D-T data. In these simulations, we specify the spherical-harmonic mode coefficients $|A_{l,m}|$ to be functions of l only, but with randomly chosen signs for each value of l and m, and we use several functional scalings for $|A_{l,m}|(l)$ in order to vary the one-dimensional power spectrum and total rms. In the simulations described in this section, we assume an isotropically emitting, nonpolarized, incoherent, broadband diffuse backlight source which subtends f/4 as viewed from the capsule center; this is comparable to current experimental configurations. In all cases, we image the midplane of the capsule with an f/4 lens having a 3-μm-diam (full width at half-maximum intensity) point-spread function.

Shadowgraph analysis is performed with LAYER (Ref. 9), the code which is also used to analyze experimental bright band data. In this analysis, the radial position of the bright band can be defined by a steepest-slope fit to either edge of the bright band or by a Gaussian centroid fit to the center of the bright band. The inside edge fit has historically been used to analyze experimental data while the Gaussian fit was only recently implemented. LAYER outputs a linearly unfolded bright-band curve and a one-dimensional bright-band-derived power spectrum in units of pixels-squared. The bright-band-derived power spectra can then be converted to units of μm-squared using the known scaling of the shadowgraph data for direct comparison to the known input ice-surface power spectrum.

Figures 3a and 3b show two simulated shadowgraphs from SHELL3D, both of which assume a 1-mm-diam capsule with a 10-μm-thick plastic shell and a 100-μm-thick D-T ice layer. Figure 3a specifies ten modes of one-dimensional (rotationally symmetric about the x-axis in Fig. 2) surface structure, while Fig. 3b specifies ten modes of two-dimensional surface structure with a comparable value for the total rms. Figures 3c and 3d show the power spectra of the actual ice surface profiles from Figs. 3a and 3b, respectively, together with bright-band-derived power spectra using both the edge fit and the Gaussian fit to define the bright-band position.

Several features are important to note in these figures. First, both the edge fit and the Gaussian fit to the bright-band position in the rotationally symmetric case of Fig. 3c yield bright-band-derived power spectra which are in excellent agreement with the known input spectrum over the ten modes which are actually present, but the edge fit diverges from the input spectrum for mode numbers >10 while the Gaussian-fit power spectrum falls rapidly above mode 10, in agreement with the input spectrum. This behavior is generally reproduced in the two-dimensional example in Fig. 3d; however, the bright-band-derived power spectra do not match the input spectrum as well over the first ten modes using either fit algorithm. We have found this to be a general feature of the two-dimensionally rough surfaces we have modeled and analyzed, and it represents a difference from the rotationally symmetric results reported earlier.[6] This poorer peak-by-peak agreement likely results from polar-angle averaging (in the z-direction of Fig. 2), which has a much stronger effect in the two-dimensionally rough case than in the rotationally symmetric case, and is dominated by the effective f/# of the diffuse backlight, as will be discussed below. We return to the reasons for the generally poorer agreement between the input spectra and the edge-fit bright-band spectra later in this section.

Recent experimental D-T ice data[11] have shown ~1.5 μm total rms roughness (modes 1 to 60) and ~0.5 μm rms roughness for modes 3 to 60, using beta layering in a 2-mm-diam capsule with a 30-μm-thick shell and a 200-μm-thick ice layer. These data were analyzed using a Gaussian centroid fit to define the bright-band position, and the results are significantly smoother than earlier data[12] (analyzed with an edge fit to define the bright-band position) appeared to indicate. We show here that the current results are almost certainly correct, and that the earlier results were in error because the edge fit analysis yields spurious high-mode power.

Figure 4a is an experimental shadowgraph of a D-T ice layer in a cryogenic capsule,[11] and Fig. 4b shows bright-band-derived power spectra from both the Gaussian centroid fit and the edge fit. The edge-fit power spectrum clearly shows higher power in the higher modes, and has an rms which is 86% higher. As noted above, the Gaussian centroid fit spectrum was expected to be correct based on earlier simulation results.[6] In order to verify this conclusion for the present case, we performed two simulations, which are shown in Figs. 4c and 4e. The first simulation is derived from a mathematical ice surface (with the same capsule and ice thickness parameters), which was specified to have a known power spectrum that nearly matches the Gaussian-fit spectrum from

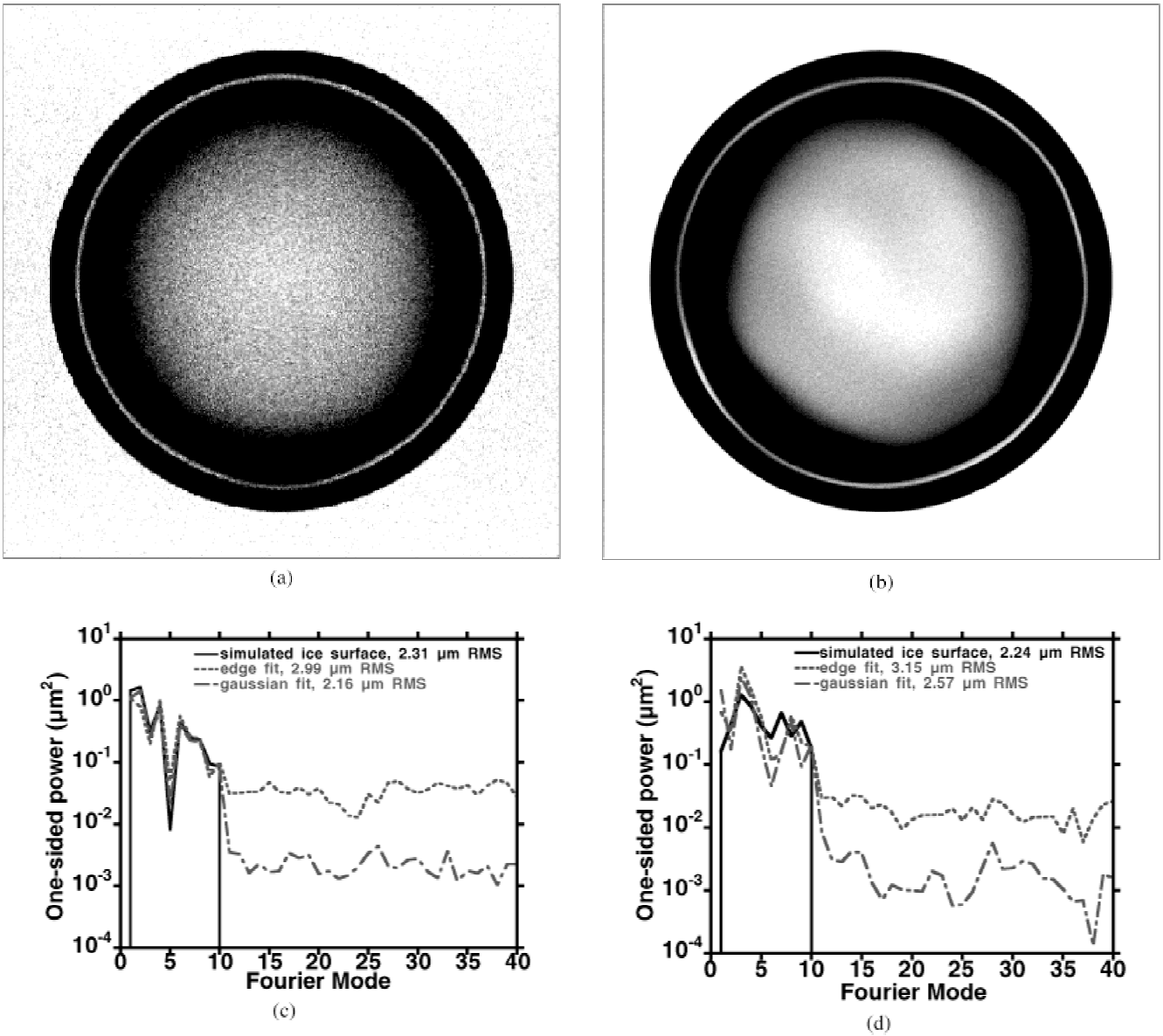

Fig. 3. (a) Simulated shadowgraph of a rotationally symmetric ice surface with ten L-modes of asymmetry; (b) simulated shadowgraph of a two-dimensionally rough ice surface with ten LM-modes of asymmetry; (c) great-circle ice surface power spectrum for the simulation of Fig. 3a together with edge-fit and Gaussian-fit bright-band power spectra; (d) great-circle ice surface power spectrum for the simulation of Fig. 3b together with edge-fit and Gaussian-fit bright-band power spectra.

Fig. 4b over the first 40 modes; the second simulation is derived from a mathematical ice surface (again with the same capsule and ice thickness parameters), which was specified to have a known power spectrum which nearly matches the edge-fit spectrum from Fig. 4b over the first 40 modes. Qualitatively, the shadowgraph in Fig. 4c appears fairly smooth, whereas the shadowgraph in Fig. 4e appears substantially more mottled than the experimental ice surface shown in Fig. 4a. This suggests that the experimental ice surface cannot be as rough as the edge-fit spectrum would indicate; this is quantitatively supported by the results from analysis of the two simulated shadowgraphs, which are shown in Figs. 4d and 4f respectively. In both cases, the Gaussian-centroid fit to the bright-band position matches the input spectrum very well, with total rms errors $<35\%$, while in both cases the edge-fit to the bright-band position seriously overestimates the power in modes >1 and overestimates the rms by factors of 1.5 to 2. We have reached similar conclusions from all other simulations we have analyzed; we therefore conclude

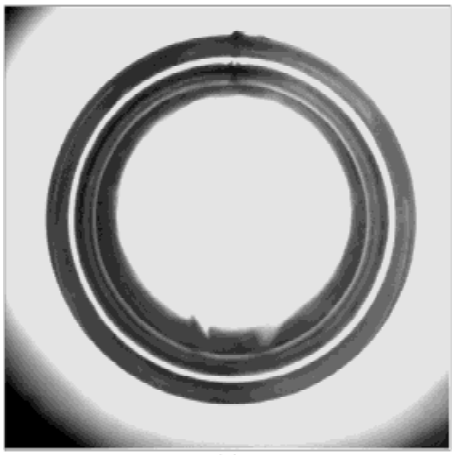

(a)

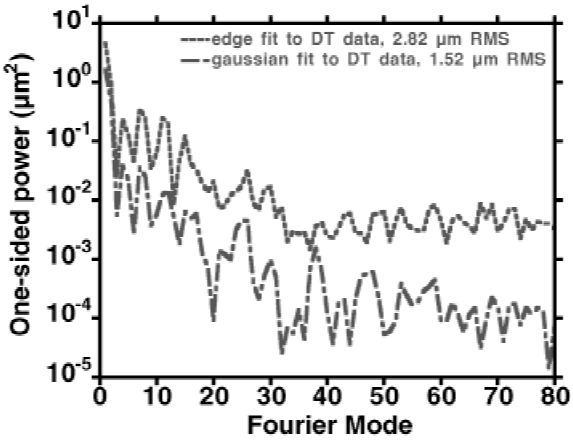

(b)

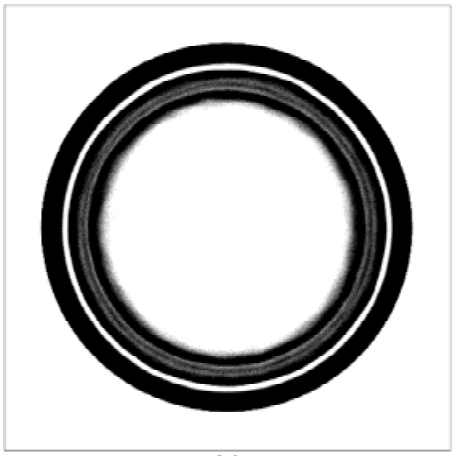

(c)

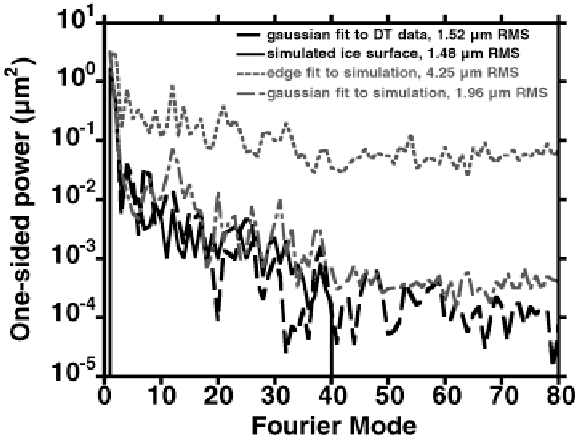

(d)

(e)

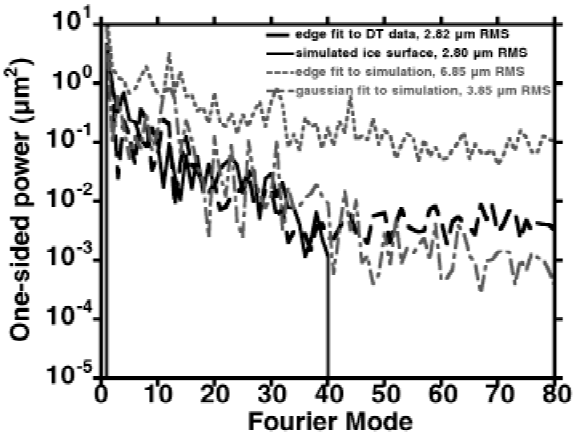

(f)

Fig. 4. (a) Experimental shadowgraph of D-T ice; (b) Edge-fit and Gaussian-fit bright-band power spectra from the data of Fig. 4a; (c) simulated shadowgraph of an ice surface with a great-circle ice surface power spectrum nearly equal to the Gaussian-fit bright-band power spectrum from the experimental data over the first 40 modes; (d) great-circle ice surface power spectrum for the simulation of Fig. 4c together with edge-fit and Gaussian-fit bright-band power spectra; (e) simulated shadowgraph of an ice surface with a great-circle ice surface power spectrum nearly equal to the edge-fit bright-band power spectrum from the experimental data over the first 40 modes; (f) great-circle ice surface power spectrum for the simulation of Fig. 4e together with edge-fit and Gaussian-fit bright-band power spectra. The shadowgraph image intensity scales have been adjusted to show the bright band and inner bands more clearly.

that the Gaussian-centroid fit to the experimental data is essentially correct and that the edge fits used to analyze older experimental data were consistently overestimating both the higher-mode power and the total rms.

There appear to be two reasons for the poor accuracy of the edge-fit analysis algorithm. First, the edge fit appears to be more susceptible to noise in the data, resulting in large spurious variations in the fitted position of the bright band. This is clear from Fig. 5, which shows a known great-circle ice surface profile for a ten-mode two-dimensionally-rough simulation (that of Fig. 3b) together with linearly unfolded shadowgraph bright bands and the corresponding Gaussian- and edge-fit profiles. The edge fit clearly shows spurious power in higher modes, which is not actually present in the simulated ice surface, while the Gaussian fit matches the known input spectrum much more closely. The reason for this difference may be related to the lack of sharp edges in the bright band which would tend to help define the bright-band position for the edge fit. Even the Gaussian fit does not exactly match the input profile, however, for reasons discussed below.

The second reason for the poorer accuracy of the edge-fit analysis is averaging along the surface in the

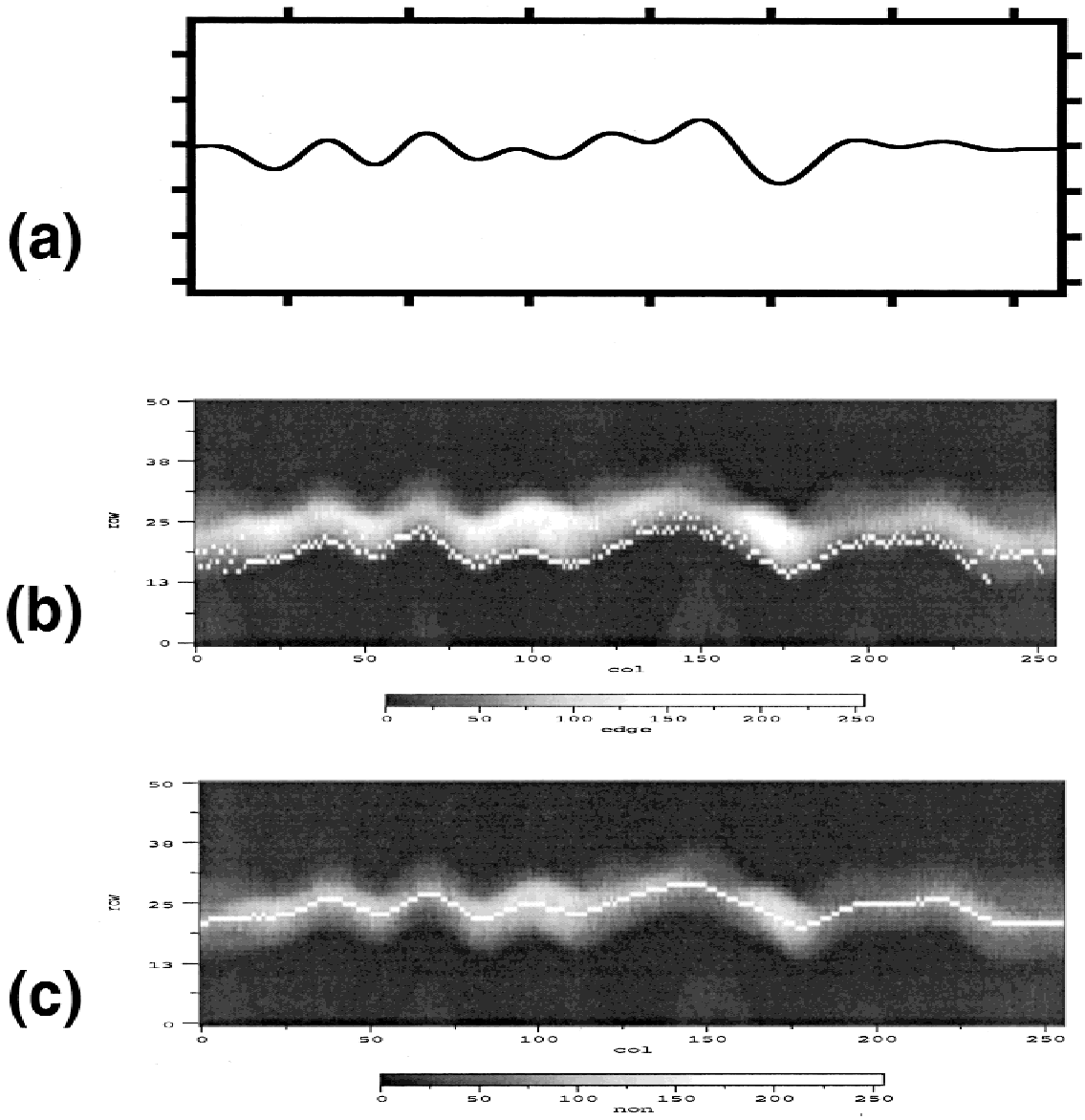

Fig. 5. (a) Great-circle ice surface profile from the 10-mode simulation of Fig. 3b; (b) unfolded bright band and edge-fit profile (thin white line) from the simulation of Fig. 3b; (c) unfolded bright band and Gaussian-fit profile (thin white line) from the simulation of Fig. 3b. The horizontal axis is azimuth angle from 0 to 360 deg, and the vertical axis is radius. The vertical scale varies in these plots.

direction of the optical axis. Figure 6 is a map of bright-band radius versus polar angle on the ice surface (relative to the z-axis in Fig. 2), showing where rays which contribute to the bright band at a particular radius have intersected the ice surface. Each radius of the bright band consists of many rays which have intersected the ice surface at various polar angles; for this example of an f/4 diffuse backlight and f/4 imaging, a particular radius in the shadowgraph bright band corresponds to light which reflects off the ice surface over a ~12-deg-wide circular ribbon symmetric about the z-axis in Fig. 2. Surface structure on the ice surface along this direction (particularly with mode numbers greater than ~30, corresponding to the 12-deg width) will therefore broaden the bright band and the edge fit will track the inner edge of this broadened distribution. This adds spurious power to higher surface modes by confusing structure in the polar direction with structure in the azimuthal direction.

This effect is illustrated in Fig. 7, which shows a known great-circle ice surface profile for a 40-mode two-dimensionally rough simulation (that of Fig. 4e) together with linearly unfolded shadowgraph bright bands and the corresponding Gaussian- and edge-fit profiles. The edge-fit tracks scattering artifacts in the bright band along the lower boundary which do not correspond to actual great-circle-plane ice surface features along the azimuth, but rather correspond to structure in the polar direction which has been averaged, resulting in a locally broadened band. The Gaussian fit, in contrast, is less affected by polar averaging, and tracks the center of the distribution regardless of its width. This averaging does affect the absolute accuracy of the Gaussian fit, however, and is likely to be the reason why the Gaussian-fit power spectrum does not exactly match the input spectrum in two-dimensionally rough simulations (this is obvious, e.g., in Fig. 5).

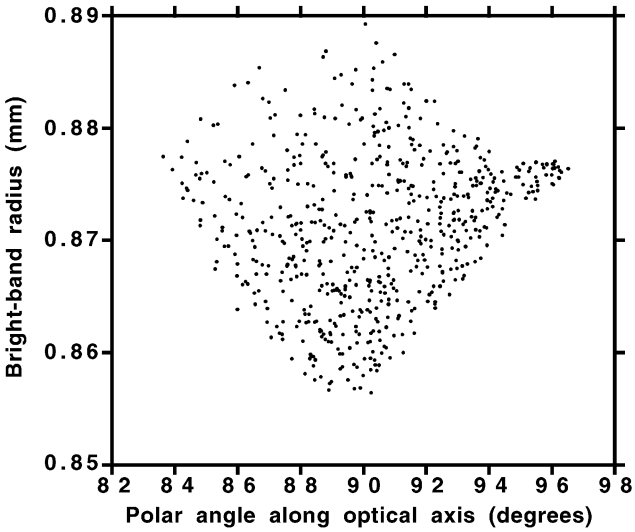

Fig. 6. Points corresponding to rays which appear at a particular radius in the bright band and which have reflected off the inner ice surface at a particular polar angle relative to the z-axis of Fig. 2. This particular example is for an f/4 diffuse backlight and f/4 imaging, a 2-mm-diam capsule, a 30-μm-thick shell, and a 150-μm-thick ice layer. The bright band clearly averages over a ~12-deg-wide circular ribbon in this case.

IV. PROGRESS TOWARD IMPROVED D-T ICE CHARACTERIZATION

Based on the simulation work described above, we believe that diffuse-backlit shadowgraphy is a valid diagnostic of currently achievable D-T ice surface power spectra for great-circle mode numbers at least as high as 40, and probably[6] as high as 80, provided a Gaussian centroid position fit is used to define the local bright-band radius. We also find that the edge-fit previously used to define the local bright-band radius yields erroneously high power and overestimates the total rms by factors as large as 2; as a corollary, we find that experimentally produced ice surfaces are smoother than were once believed.

Despite these successes, there are several reasons to seek improved optical metrology techniques. Imaging with a diffuse backlight naturally increases polar averaging and eliminates any one-to-one correspondence between bright-band position and ice thickness in a single perpendicular plane (see Fig. 6). This averaging broadens the bright band, degrades the achievable position-fitting precision, and limits our ability to observe and diagnose short scale-length features. In addition, extremely smooth ice surfaces will become increasingly difficult to quantitatively diagnose since the radial variations in the bright-band position will become too small to observe. Finally, we anticipate a need to characterize D-T ice surfaces in situ, in a cylindrical radiation case (a hohlraum) in the NIF target chamber prior to an ignition experiment, and restricted access to the capsule will constrain our ability to utilize existing characterization techniques.

One simple improvement to current backlit shadowgraphy is to use a collimated backlight rather than a diffuse backlight. Figure 8 shows SHELL3D simulated sections of a bright band which would be observed from the same ice surface under f/4 diffuse backlight conditions and under collimated (e.g., laser) backlight conditions. The collimated-backlight geometry clearly produces a sharper bright band, the position of which can be defined more precisely. Perhaps more importantly, however, the effects of polar averaging are minimized in the case of a collimated backlight, and a one-to-one relationship can be identified between ice surface features in a single perpendicular plane and features in the bright band, particularly along the outer edge (see Fig. 9). This suggests

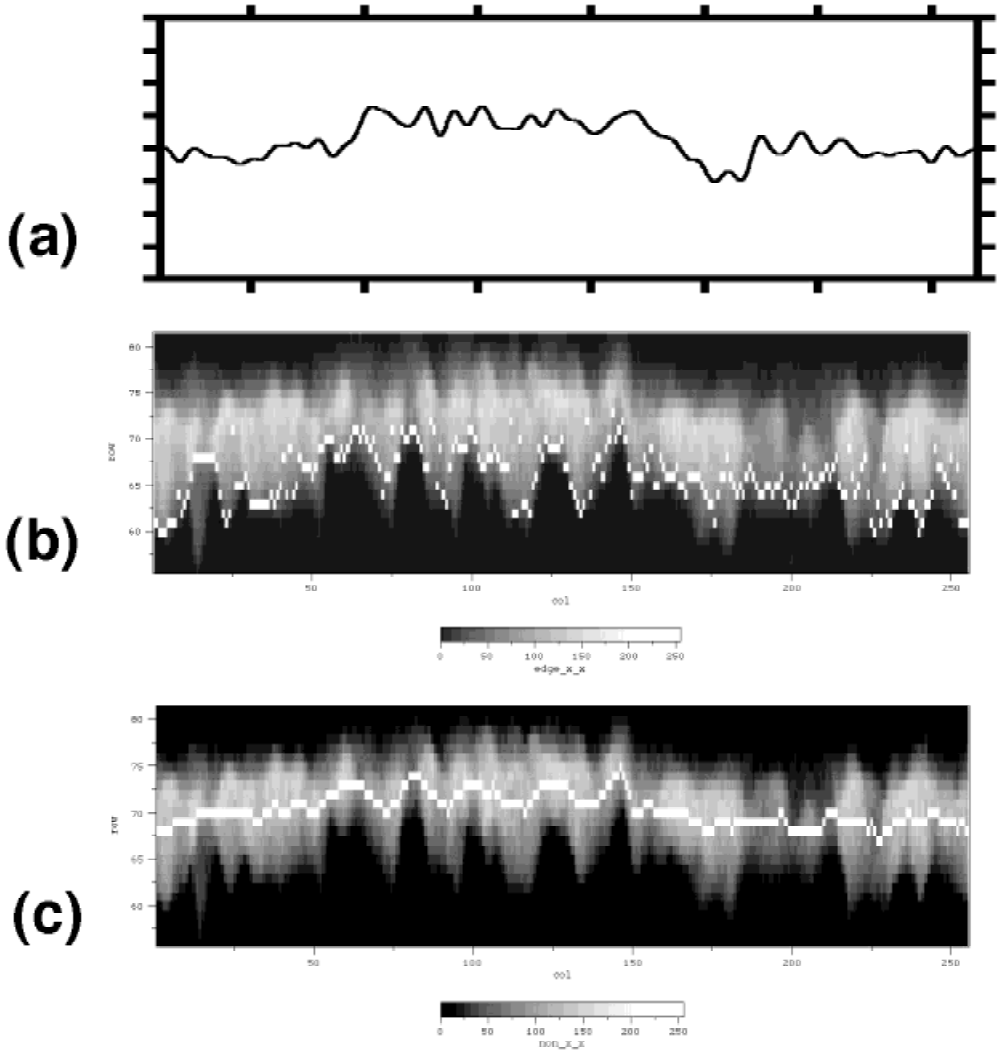

Fig. 7. (a) Great-circle ice surface profile from the 40-mode simulation of Fig. 4e; (b) unfolded bright band and edge-fit profile from the simulation of Fig. 4e; (c) unfolded bright band and Gaussian-fit profile from the simulation of Fig. 4e.

that higher-frequency spatial structure will be more easily observed at the outer edge of the bright band using a collimated backlight geometry, provided the ice surface quality is sufficiently good to avoid bifurcations such as those apparent in Fig. 8.

We also note that most shadowgraphs (e.g., Fig. 4c and 4e) clearly show inner bands which are weaker but more distorted than the bright band. These bands result from other multiple-reflection ray paths, and appear visually to be more sensitive indicators of ice-surface asymmetry than the bright band itself; however, the more complicated ray paths suggest that discerning a quantitative correspondence between inner-band structure and ice surface structure will be challenging. Additionally, the central portions of the shadowgraphs (e.g., in Fig. 3b) show mottled structure which is clearly related to ice surface asymmetry; this structure may provide additional surface-quality information (particularly with a collimated backlight), though again the quantitative correspondence will probably be difficult to discern.

Finally, we note that bright-band transmission interferometry might be utilized to provide ice surface-quality information. A simple implementation of this technique would be to interfere a plane-wave reference beam with a collimated-backlight shadowgraph image; in this case, the ray paths are already understood from the above analysis, and the quantitative correspondence between bright-band phase and surface structure is straightforward to derive for a given shell thickness, nominal ice thickness, and capsule diameter. In Fig. 10 we show a simulated bright-band interferogram, obtained by interfering a shadowgraph image (that of Fig. 3b) with a plane-parallel reference beam. The bright-band phase varies significantly in azimuth and radius, and this

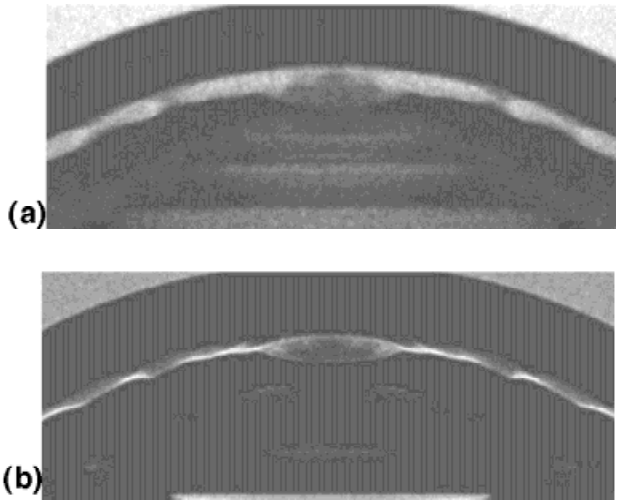

Fig. 8. Segment of the bright-band structure; (a) uses a diffuse backlight, while (b) uses a collimated backlight. The collimated backlight produces a sharper bright band, the position of which can be more precisely defined.

phase correlates to the same surface structure which affects the radial position of the peak bright-band intensity (in this particular case, one wave of phase corresponds to 1.4 μm of ice-thickness radial variation). These phase

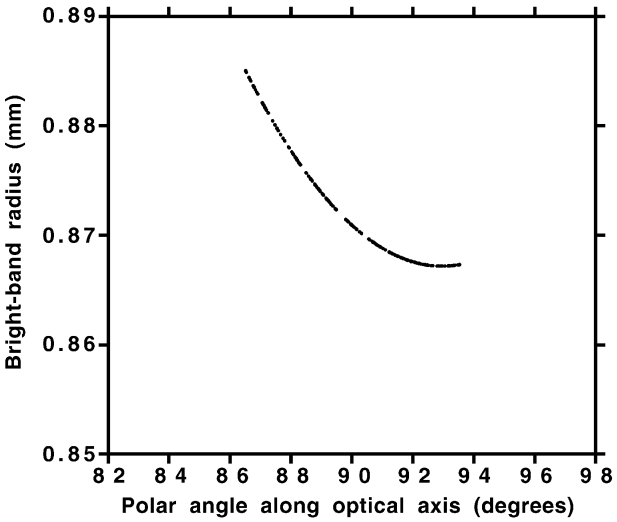

Fig. 9. Points corresponding to rays which appear at a particular radius in the bright band and which have reflected off the inner ice surface at a particular polar angle relative to the z-axis of Fig. 2. This particular example is for a collimated backlight and f/4 imaging, a 2-mm-diam capsule, a 30-μm-thick shell, and a 150-μm-thick ice layer. The inner edge of the bright band averages over a ~3-deg-wide circular ribbon in this case, while the outer edge of the bright band tracks a single trace along the ice surface.

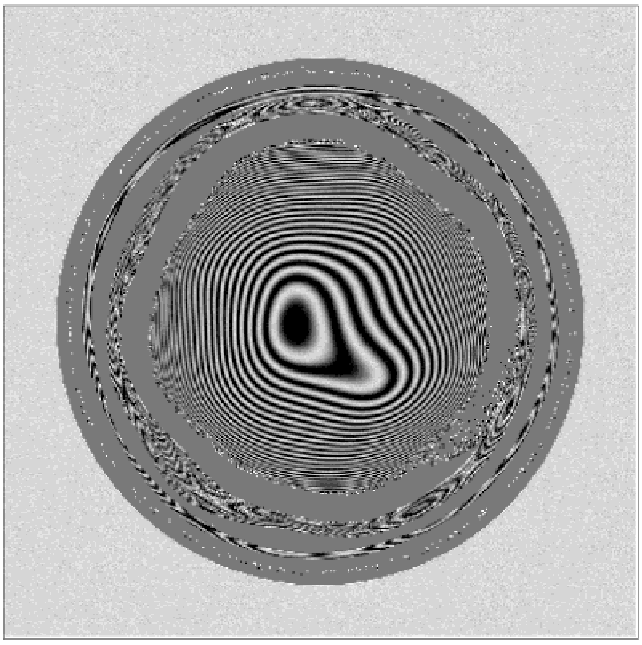

Fig. 10. Simulated transmission interferogram of a two-dimensionally rough ice surface with 10 LM-modes of asymmetry, using a collimated backlight but otherwise using the same model parameters as used for the simulated diffuse-backlight shadowgraph shown in Fig. 3b. Phase information in the bright band relates to optical path length difference; this can be related to surface roughness and can perhaps be observed more easily than radial position variations.

variations may be more easily measured than radial variations of the position of the bright band, particularly for cases where the ice surface is nearly perfect. We are working toward developing phase unwrapping software which can be used to analyze bright-band interferograms, and we hope to perform experiments to develop this and other ice surface characterization techniques in the near future.

V. SUMMARY AND CONCLUSIONS

In summary, we have developed a numerical raytrace model to investigate backlit imaging of a transparent spherical shell having a lower-index ice layer adhering its inner surface. This geometry corresponds to future ICF ignition targets, where a D-T ice layer is contained within a spherical ablator shell. This application places stringent demands upon the surface quality of the D-T ice layer, and we have used our raytrace model to quantify the limitations of backlit shadowgraphy as a diagnostic of the quality of this ice surface. We find that conventional diffuse-backlit shadowgraphy is a reliable diagnostic of the mode spectrum of ice-surface

imperfections for mode numbers as high as 80 provided the radial position of the TIR bright band, formed by light reflecting off the inner ice surface at grazing angles of incidence, is defined with a Gaussian centroid fit, and we use our model to investigate the limitations of the technique due to bright-band position fitting errors and due to polar averaging related to the numerical aperture of the diffuse backlight. We also explore various alternative optical metrology diagnostics based upon backlit imaging, and we suggest that improved diagnostic accuracy might be obtained using a small numerical-aperture backlight and by making use of information contained in other parts of the backlit image. Finally, we suggest that backlit optical interferometry may be a very sensitive metrology tool for this application, and we present simulated wrapped-phase maps illustrating the principle.

ACKNOWLEDGMENTS

We thank J. Burmann, E. M. Campbell, S. Haan, J. Hoffer, R. Jones, B. Kozioziemski, E. Mapoles, J. Pipes, and W. Unites for their contributions and support. This work was performed under the auspices of the U.S. Department of Energy by the University of California Lawrence Livermore National Laboratory under contract W-7405-ENG-48.

REFERENCES

1. J. D. LINDL, *Inertial Confinement Fusion*, Springer-Verlag, New York (1998).

2. T. R. DITTRICH, S. W. HAAN, M. M. MARINAK, S. M. POLLAINE, and R. McEACHERN, "Reduced Scale National Ignition Facility Capsule Design," *Phys. Plasmas*, **5**, 3708 (1998).

3. T. R. DITTRICH, S. W. HAAN, M. M. MARINAK, S. M. POLLAINE, D. E. HINKEL, D. H. MUNRO, C. P. VERDON, G. L. STROBEL, R. McEACHERN, R. C. COOK, C. C. ROBERTS, D. C. WILSON, P. A. BRADLEY, L. R. FOREMAN, and W. S. VARNUM, "Review of Indirect-Drive Ignition Design Options for the National Ignition Facility," *Phys. Plasmas*, **6**, 2164 (1999).

4. J. K. HOFFER, L. R. FOREMAN, J. J. SANCHEZ, E. R. MAPOLES, and J. D. SHELIAK, "Surface Roughness Measurements of Beta-Layered Solid Deuterium-Tritium in Toroidal Geometries," *Fusion Technol.*, **30**, 529 (1996).

5. Y. LEE, Personal Communication.

6. J. A. KOCH, T. P. BERNAT, G. W. COLLINS, B. A. HAMMEL, B. J. KOZIOZIEMSKI, A. J. MacKINNON, J. D. SATER, D. N. BITTNER, and Y. LEE, "Quantitative Analysis of Backlit Shadowgraphy as a Diagnostic of Hydrogen Ice Surface Quality in ICF Capsules," *Fusion Technol.*, **38**, 123 (2000).

7. E. BUTKOV, *Mathematical Physics*, Addison-Wesley, Reading, Massachusetts (1968).

8. W. H. PRESS, S. A. TEUKOLSKY, W. T. VETTERLING, and B. P. FLANNERY, *Numerical Recipes in C*, Cambridge University Press, Cambridge, United Kingdom (1994).

9. E. R. MAPOLES, J. SATER, J. PIPES, and E. MONSLER, "Smoothing of Deuterium-Tritium Ice by Electrical Heating of the Saturated Vapor," *Phys. Rev. E*, **55**, 3473 (1997).

10. S. M. POLLAINE, S. P. HATCHETT, and S. H. LANGER, "Spectral Analysis of ICF Capsule Surfaces," 1994 ICF Annual Report, Report UCRL-LR-105820-94, Lawrence Livermore National Laboratory (June 1995).

11. J. D. SATER, Data from LLNL D-T ice experiments (unpublished).

12. J. SATER, B. KOZIOZIEMSKI, G. W. COLLINS, E. R. MAPOLES, J. PIPES, J. BURMANN, and T. P. BERNAT, "Cryogenic D-T Fuel Layers Formed in 1 mm Spheres by Beta-Layering," *Fusion Technol.*, **35**, 229 (1999).

Jeffrey A. Koch (BS, Michigan State University, 1988; PhD, University of California, Davis, 1993) is a physicist at Lawrence Livermore National Laboratory and is currently group leader for implosion physics in the Target Ignition Physics Program. His research interests span a wide range of laser produced-plasma related topics.

Thomas P. Bernat (BA, Claremont McKenna College, 1966; PhD, Brandeis University, 1972) is a physicist at Lawrence Livermore National Laboratory, where he is associate program leader for Target Science and Technology in the Inertial Confinement Fusion Program. His research interests are in the areas of condensed matter physics and ignition target development.

Gilbert W. Collins (BS, University of Cincinnati, 1983; PhD, Ohio State University, 1989) is currently shock physics group leader in the inertial confinement fusion program. His research interests include investigating matter under extreme densities and pressure, shock physics, inertial confinement fusion, hydrodynamics, and diffusion mechanisms in quantum solids.

Bruce A. Hammel (BA, physics, University of California, Berkeley, 1977; PhD, astrophysical, planetary and atmospheric sciences, University of Colorado, Boulder, 1984) is a physicist at Lawrence Livermore National Laboratory and is currently the program leader for Target Ignition Physics. His research interests are in the areas of hydrodynamics, radiative properties of hot dense matter, short pulse laser matter interaction, and Inertial Confinement Fusion.

Andrew J. MacKinnon (BS, Heriot-Watt University, Edinburgh, United Kingdom, 1988; PhD, Imperial College, London University, United Kingdom, 1996) is a physicist at Lawrence Livermore National Laboratory, and is currently in the Inertial Confinement Fusion Program. His main research interests are in high intensity laser matter interactions, including laser propagation in plasmas and particle acceleration.

Charles H. Still (BS, 1984, PhD, 1990, University of South Carolina) is a computational physicist at Lawrence Livermore National Laboratory in the Plasma Physics Theory Group of X-Division, Defense and Nuclear Technologies Directorate and the Inertial Confinement Fusion Program. His research interests are laser-plasma interactions and their simulation.

James D. Sater (BS, University of Missouri, Rolla, 1980; PhD, Ohio State University, 1988) is a physicist with Schafer Corporation, and is the leader of the Schafer cryogenics group. His research is focused on solid properties of deuterium-tritide near the triple point.

Donald N. Bittner (BS, University of Pittsburgh, 1975; MS, University of Michigan, 1978; PhD, University of Michigan, 1984) is a senior scientist at Schafer Corporation. His research interests include investigating the properties of materials at low temperatures.